A New Class of Wideband Multisection 180° Hybrid Rings Using Vertically Installed Planar Couplers

Chun-Hsiang Chi and Chi-Yang Chang, *Member, IEEE*

***Abstract*—A new class of wideband multisection 180° hybrid rings using the vertically installed planar (VIP) coupler is proposed. On the basis of the reconfigured ideal single-section 180° hybrid ring (i.e., the 180° hybrid ring with an ideal phase inverter), the multisection 180° hybrid rings can be realized by properly cascading of single-section 180° hybrid rings. Compared with the conventional hybrid ring, the two-section hybrid rings exhibit wide bandwidth, size reduction, and easily achievable high power-division ratios. Design equations based on the equal-ripple functions are derived. Design curves for the equal and unequal power-division ratio are also described. In addition, a cascade of single-section cascadable hybrid rings with a unit element at each I/O port can be used for bandwidth enhancement. Good agreement is obtained between the experimental and simulated results.**

***Index Terms*—Multisection 180° hybrid ring, phase inverter, vertically installed planar (VIP) coupler, wideband 180° hybrid ring.**

I. Introduction

THE 180° hybrid ring coupler is an important and fundamental component in microwave circuit applications such as balanced mixers, push–pull amplifiers, phase shifters, and feeding networks of antenna arrays. In the conventional hybrid ring, the 180° phase shifter is implemented by a $\lambda/2$ transmission line and its phase-shift is only 180° at the center frequency. Therefore, the conventional hybrid ring using a $3\lambda/4$ line section results in large size and narrow bandwidth. In addition, it requires a quite high impedance line for large power-division ratios. There are many approaches to overcome these limitations [1]–[5]. March [1] replaced the $3\lambda/4$ transmission line with an opposing-end short-circuited $\lambda/4$ coupled line (we simply call it the "short-ended coupled line") to increase the bandwidth of the hybrid ring. A theory of cascading of several quarter-wave transmission-line sections to each I/O port of an ideal 180° hybrid ring for bandwidth improvement has been proposed by Rehnmark [2]. Chang *et al.* [3] have proposed a method to implement the hybrid ring proposed in [2]. However, to implement these hybrid rings requires extremely low and/or high impedance lines or extremely tight coupled lines, especially for large power-division ratio situations. To reduce the impedance values, the $3\lambda/4$ line section of the hybrid ring can be split into three $\lambda/4$ lines [4]. However, the required high impedance values still increase with power-division ratios. Therefore, the realizable highest and/or lowest impedance values limit the achievable power-division ratios of those hybrid rings proposed in [1]–[4].

The 90° branch-line coupler [6] realized with a multisection structure for bandwidth enhancement is well known. The multisection 180° hybrid ring was first proposed by Ang *et al.* [5] to achieve broad bandwidth and high power-division ratios. However, because each single-section unit in [5] was based on the conventional hybrid ring with the narrow-band phase inverter, the amplitude and the phase performances of two output ports cannot achieve broad bandwidth simultaneously. Therefore, in [5], only conditions at the center frequency are derived, and the responses out of the center frequency have not been discussed analytically. In addition, the bandwidth of the hybrid ring will dramatically decrease with increasing of power-division ratios.

In this paper, the multisection 180° hybrid rings are presented to overcome the above shortcomings. The basic building block of the proposed multisection 180° hybrid ring is the reconfigured ideal 180° hybrid ring, as shown in Fig. 1(a) and (b). The proposed single-section hybrid ring can be easily cascaded like the 90° branch-line coupler, as depicted in Fig. 1(c). The reconfiguration proposed in Fig. 1(b) results in size reduction. Furthermore, the hybrid ring in Fig. 1(b) with two output ports on the same side is convenient for the applications such as the balanced mixer or the push–pull amplifier. Synthesis procedures to realize the Chebyshev-response two-section cascaded 180° hybrid rings shown in Fig. 1(c) with various power-division ratios will be described. The reconfigured single-section 180° hybrid ring with a unit element at each port [2], [3] can be cascaded to exhibit extended bandwidth as shown in Fig. 2. As an example, the 3-dB two-section hybrid ring with 15-dB return loss yields a bandwidth of 5:1. However, the realization of a broadband phase inverter on microstrip circuits could be a problem. Fortunately, as described in [1] that a short-ended $\lambda/4$ coupled line can provide 270° phase shift, and the ratio of the even- and odd-mode impedance of the coupled line determines the bandwidth. The higher even-to-odd-mode impedance ratio produces wider bandwidth. As the ratio approaches an asymptotic value, the short-ended coupled line is equivalent to a $\lambda/4$ line cascaded with an ideal phase inverter. To achieve enough bandwidth, a very tight coupled line must be implemented. In this paper, the VIP coupler described in [7] is proposed to implement the very tight coupled lines. With the VIP coupler, the proposed wideband multisection hybrid rings can be easily implemented by microstrip circuits. Several design examples show that the proposed multisection 180° hybrid rings not only exhibit broad bandwidth but also depict a wide range of power-division ratios.

Manuscript received November 21, 2005; revised January 24, 2006. This work was supported in part by the National Science Council, R.O.C., under Grant NSC 95-2752-E-009-003-PAE.

The authors are with the Department of Communication Engineering, National Chiao Tung University, Hsinchu City 300, Taiwan, R.O.C. (e-mail: kavh.cm91g@nctu.edu.tw; mhchang@cc.nctu.edu.tw).

Digital Object Identifier 10.1109/TMTT.2006.875799

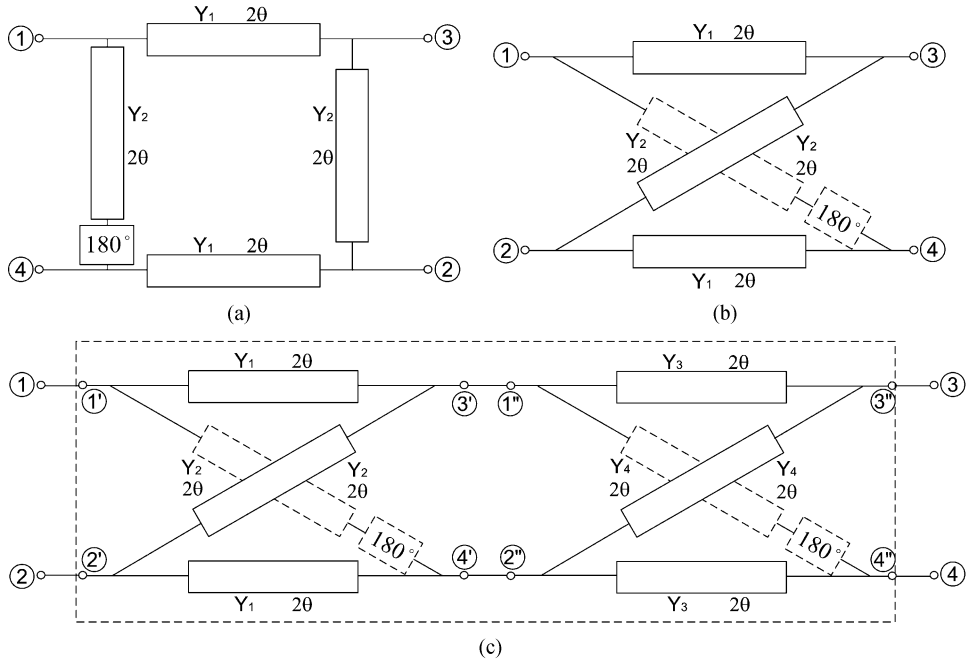

Fig. 1. Schematics of hybrid rings using an ideal phase inverter (a) Conventional hybrid ring. (b) Reconfigured hybrid ring. (c) Proposed two-section hybrid ring.

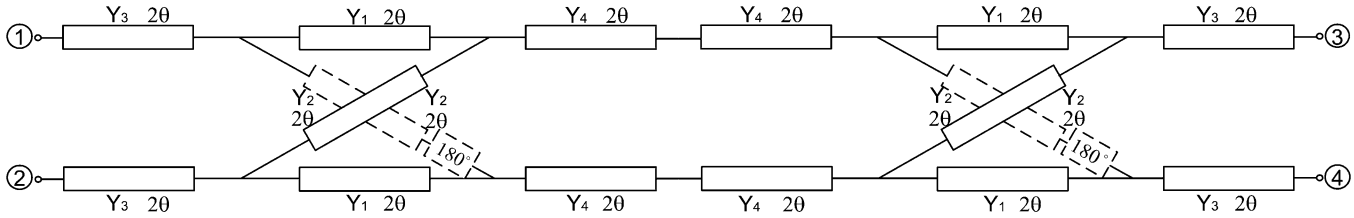

Fig. 2. Schematic of the proposed two-section hybrid ring with a unit element at each I/O port.

II. Theoretical Analysis of The Two-Section Hybrid Ring

In the reconfigured single-section hybrid ring shown Fig. 1(b), the admittance Y_1 and Y_2 are normalized values with respect to system admittance Y_0. Using the even- and odd-mode analysis, the ABCD matrices for the even- and odd-mode cascade element are given by

$$\begin{bmatrix} A_e & B_e \\ C_e & D_e \end{bmatrix} = \frac{1}{(1-t^2)} \begin{bmatrix} A_1(t^2) & tB_0(t^2) \\ \frac{1}{t}C_2(t^2) & D_1(t^2) \end{bmatrix} = \begin{bmatrix} A & B \\ C & D \end{bmatrix} \quad (1)$$

$$\begin{bmatrix} A_o & B_o \\ C_o & D_o \end{bmatrix} = \begin{bmatrix} D_e & B_e \\ C_e & A_e \end{bmatrix} = \begin{bmatrix} D & B \\ C & A \end{bmatrix} \quad (2)$$

where $t = j\tan\theta$ and the subscripts indicate the degree of the polynomials $A(t^2), B(t^2), C(t^2)$, and $D(t^2)$. Therefore, the S-parameters of the single-section hybrid ring can be expressed as

$$\begin{aligned} S_{11s} &= S_{22s} \\ &= \frac{B-C}{A+B+C+D} \\ S_{21s} &= 0 \\ S_{31s} &= S_{42s} \\ &= \frac{2}{A+B+C+D} \\ S_{32s} &= \frac{A-D}{A+B+C+D} \\ &= \frac{2(Y_2/Y_1)}{A+B+C+D} \\ S_{41s} &= \frac{D-A}{A+B+C+D} \\ &= \frac{-2(Y_2/Y_1)}{A+B+C+D}. \end{aligned} \quad (3)$$

The conventional even- and odd- mode analysis method to obtain the S-parameters of the cascaded 90° hybrid ring [6] cannot be used in this newly proposed two-section hybrid ring

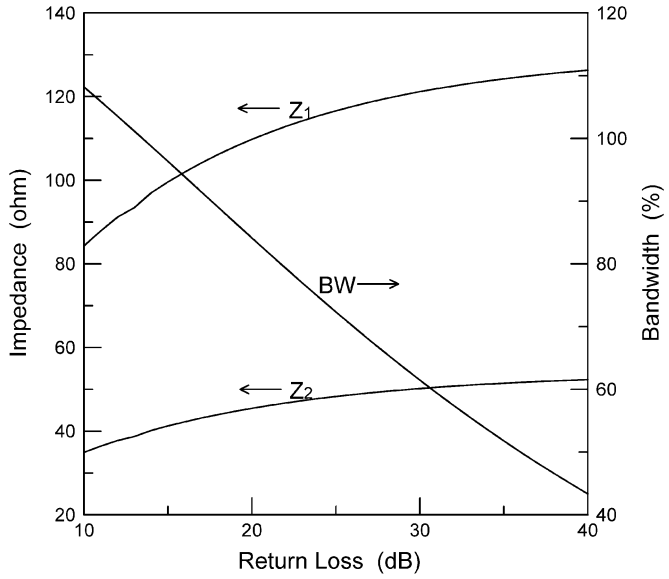

Fig. 3. Characteristic impedances Z_1, Z_2, and bandwidth versus return loss for the equal-ripple response 3-dB two-section hybrid ring.

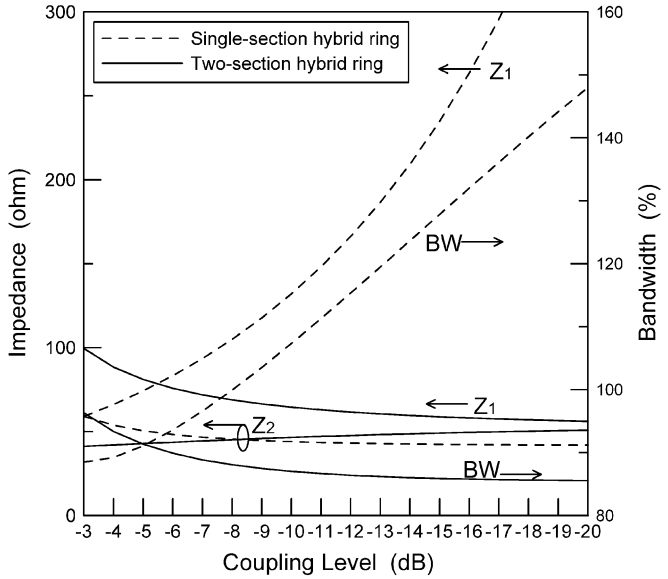

Fig. 4. Characteristic impedances Z_1, Z_2, and bandwidth versus coupling level for the single- and two-section hybrid rings with 15-dB equal-ripple return loss.

shown in Fig. 1(c) because the symmetrical planes for even- and odd-mode excitation are not exist. Here, the multiport connection method [8] is used. The results at the center frequency are shown as follows:

$$\begin{aligned}
S_{11} &= S_{22} \\
&= -S_{33} \\
&= -S_{44} \\
&= \frac{\left(Y_3^2+Y_4^2\right)-\left(Y_1^2+Y_2^2\right)}{Y_1^2+Y_2^2+Y_3^2+Y_4^2} \\
S_{21} &= 0 \\
S_{31} &= -\frac{2(Y_1Y_3-Y_2Y_4)}{Y_1^2+Y_2^2+Y_3^2+Y_4^2} \\
S_{41} &= \frac{2(Y_2Y_3+Y_1Y_4)}{Y_1^2+Y_2^2+Y_3^2+Y_4^2} \\
S_{32} &= -\frac{2(Y_2Y_3+Y_1Y_4)}{Y_1^2+Y_2^2+Y_3^2+Y_4^2} \\
S_{42} &= -\frac{2(Y_1Y_3-Y_2Y_4)}{Y_1^2+Y_2^2+Y_3^2+Y_4^2}.
\end{aligned} \tag{4}$$

When $Y_1 = Y_3$ and $Y_2 = Y_4$, all ports can be perfectly matched and the signal incident at the input port will be split between ports 3 and 4. Although all ports can be perfectly matched for the case of $Y_1 = Y_4$ and $Y_2 = Y_3$, a 0-dB coupler, which means that no signal can be obtained from one of the output ports, is obtained. Therefore, we concentrate our attention on the case of $Y_1 = Y_3$ and $Y_2 = Y_4$. Because in this case the two-section hybrid ring consists of two identical single-section hybrid rings, the synthesis procedure can be largely simplified. Again, applying the multiport connection method to (3), we obtain (5a), shown at the bottom of this page, and

$$S_{21} = 0 \tag{5b}$$

$$\begin{aligned}
S_{31} &= -\frac{(A-D)^2-4}{(A+2B+D)(A+2C+D)} \\
&= -\frac{4(Y_2/Y_1)^2-4}{(A+2B+D)(A+2C+D)}
\end{aligned} \tag{5c}$$

$$\begin{aligned}
S_{41} &= -\frac{4(A-D)}{(A+2B+D)(A+2C+D)} \\
&= -\frac{8(Y_2/Y_1)}{(A+2B+D)(A+2C+D)}
\end{aligned} \tag{5d}$$

$$\begin{aligned}
S_{32} &= \frac{4(A-D)}{(A+2B+D)(A+2C+D)} \\
&= \frac{8(Y_2/Y_1)}{(A+2B+D)(A+2C+D)}
\end{aligned} \tag{5e}$$

$$\begin{aligned}
S_{42} &= -\frac{(A-D)^2-4}{(A+2B+D)(A+2C+D)} \\
&= -\frac{4(Y_2/Y_1)^2-4}{(A+2B+D)(A+2C+D)}.
\end{aligned} \tag{5f}$$

It should be noted that the interchange between Y_1 and Y_2 results in the interchange between the sum port and the delta port. Assuming that the input is matched well in the passband, we have

$$|S_{31}|^2 + |S_{41}|^2 \approx 1. \tag{6}$$

$$S_{11} = \frac{2[B^2(A+2C+D)+B(2+A^2-2C^2+D^2)-C(2+A^2+AC+CD+D^2)]}{(A+B+C+D)(A+2B+D)(A+2C+D)} \tag{5a}$$

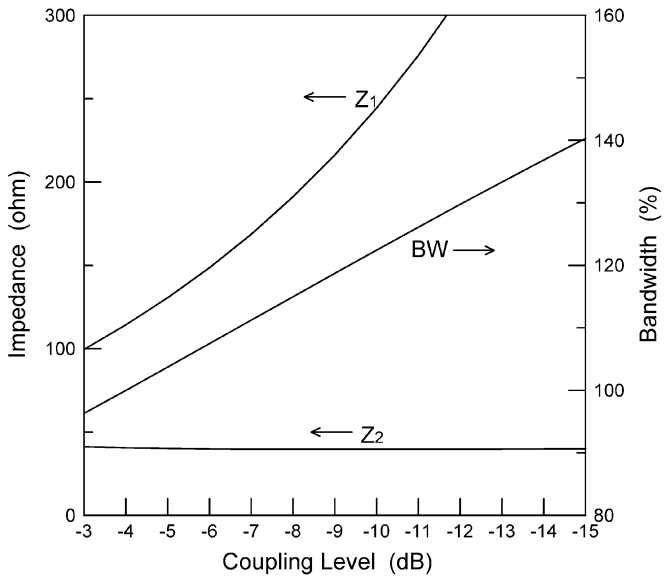

Fig. 5. Another set of characteristic impedances Z_1, Z_2, and bandwidth versus coupling level for the two-section hybrid rings with 15-dB equal-ripple return loss.

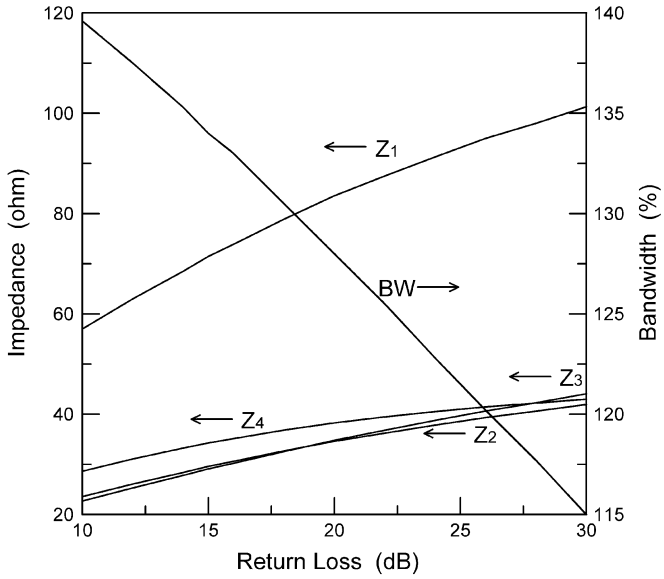

Fig. 6. Characteristic impedances Z_1, Z_2, Z_3, Z_4, and bandwidth versus return loss for the equal-ripple response 3-dB two-section hybrid ring with a unit element at each I/O port.

The output power-division ratio is

$$R = \frac{|S_{41}|^2}{|S_{31}|^2} = \left(\frac{2(Y_2/Y_1)}{(Y_2/Y_1)^2 - 1}\right)^2 \tag{7}$$

and (6) can be written as

$$|S_{31}|\sqrt{1+R} \approx 1. \tag{8}$$

Now, considering the function

$$F = \frac{|S_{11}|}{|S_{31}|\sqrt{1+R}} \tag{9}$$

where F is approximately equivalent to the reflection coefficient of the two-section hybrid ring over the passband because the denominator is very close to unity [see (8)]. Therefore, the insertion loss function P_L can be shown as given in (10), shown at the bottom of this page. As described by Riblet [9] and Carlin and Kohler [10], the insertion loss function of a Chebyshev response has the form given by (11), shown at the bottom of this page, where $\mathrm{x} = \cos 2\theta, \mathrm{x_c} = \cos 2\theta_\mathrm{c}, \mathrm{T_n(x)}$ is the Chebyshev polynomial of the first kind of degree n, and m is the parameter

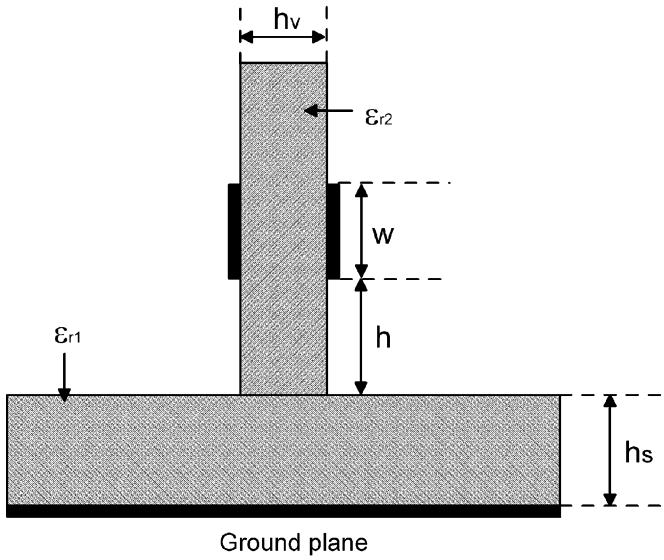

Fig. 7. Cross-sectional view of the VIP coupler.

$$P_L = 1 + |F|^2 = 1 + \left|\frac{2[B^2(A+2C+D) + B(2+A^2-2C^2+D^2) - C(2+A^2+AC+CD+D^2)]}{\sqrt{1+R}(A+B+C+D)[(A-D)^2-4]}\right|^2 \tag{10}$$

$$P_L = 1 + m^2\left\{\frac{\left(1+\sqrt{1-x_c^2}\right)T_n(x/x_c) - \left(1-\sqrt{1-x_c^2}\right)T_{n-2}(x/x_c)}{2\sqrt{1-x^2}}\right\}^2 \tag{11}$$

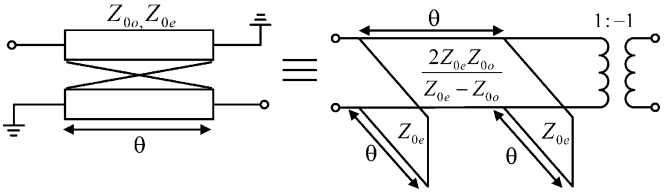

Fig. 8. Equivalent circuit of a short-ended coupled line.

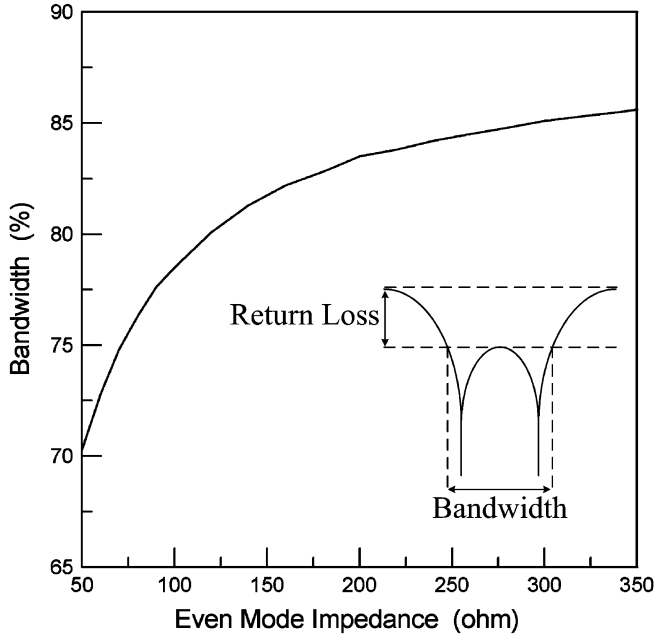

Fig. 9. Simulated 15-dB equal-ripple return loss bandwidth of a 3-dB single-section hybrid ring with a short-ended coupler versus different Z_{0e}.

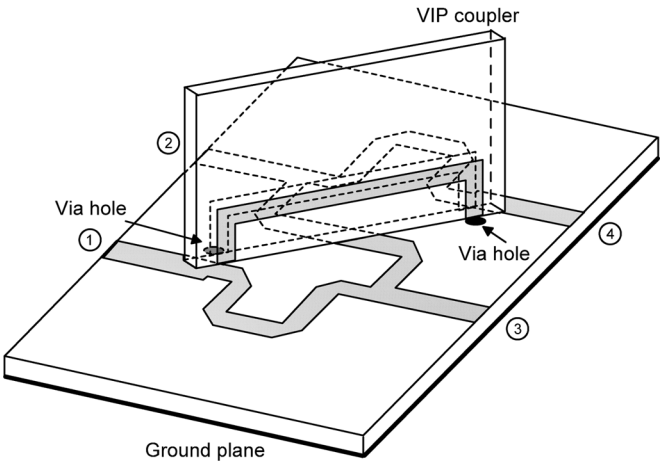

Fig. 10. 3-D structure of the single-section hybrid ring using the VIP coupler.

to control the ripple level. Substituting A, B, C, and D in (1) into (10) and fitting (10) to (11) with $n = 3$, we obtain

$$\frac{(Y_1+Y_2)\left(1-Y_1^2-Y_2^2\right)}{Y_1^2\left[\left(\frac{Y_2}{Y_1}\right)^2-1\right]\sqrt{1+R}} = m\left(\frac{2}{x_c}+\frac{\sqrt{1-x_c^2}}{x_c}\right) \tag{12}$$

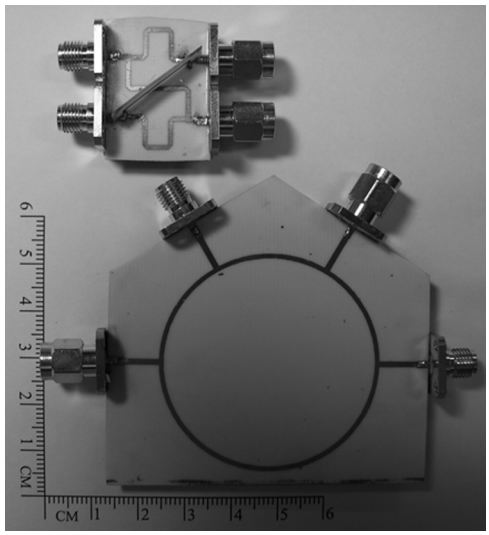

Fig. 11. Fabricated circuits of the conventional and reconfigured single-section hybrid rings.

TABLE I
VIP COUPLER PARAMETERS EXTRACTED BY HFSS ($f_0 = 2$ GHz)

Z (Ω)	h (mil)	W (mil)	ε_{re}	ε_{ro}	Z_{0e} (Ω)	Z_{0o} (Ω)	L (mil)
59.0	70	21.5	1.28	2.87	348.0	27.2	894.0
50.8	70	25.9	1.26	2.91	336.0	23.5	886.0
41.3	70	34.0	1.24	2.97	320.6	19.4	875.5
29.8	70	49.0	1.22	3.04	297.5	14.2	862.0

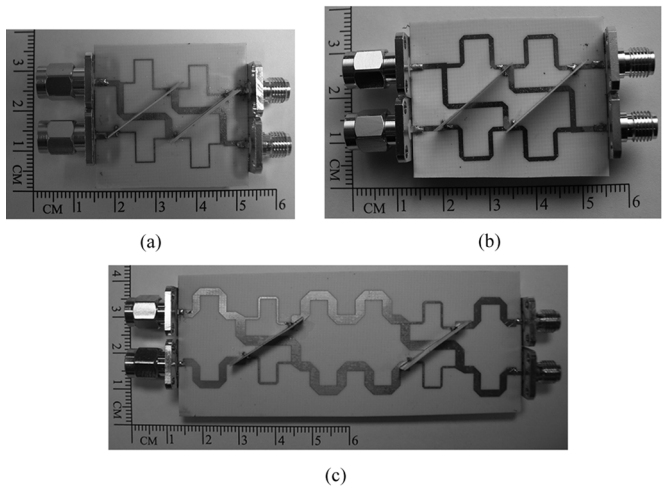

Fig. 12. Fabricated two-section hybrid rings. (a) 3-dB hybrid ring. (b) 20-dB hybrid ring. (c) 3-dB hybrid ring with a unit element at each I/O port.

$$\frac{(Y_1+Y_2)\left(-1+Y_1^2+2Y_1Y_2+Y_2^2\right)}{Y_1^2\left[\left(\frac{Y_2}{Y_1}\right)^2-1\right]\sqrt{1+R}} = -m\left(\frac{2}{x_c^3}+\frac{2\sqrt{1-x_c^2}}{x_c^3}\right). \tag{13}$$

The relationship between m and return loss is

$$\mathrm{RL} = 10\log(1+1/m^2)\,\mathrm{dB}. \tag{14}$$

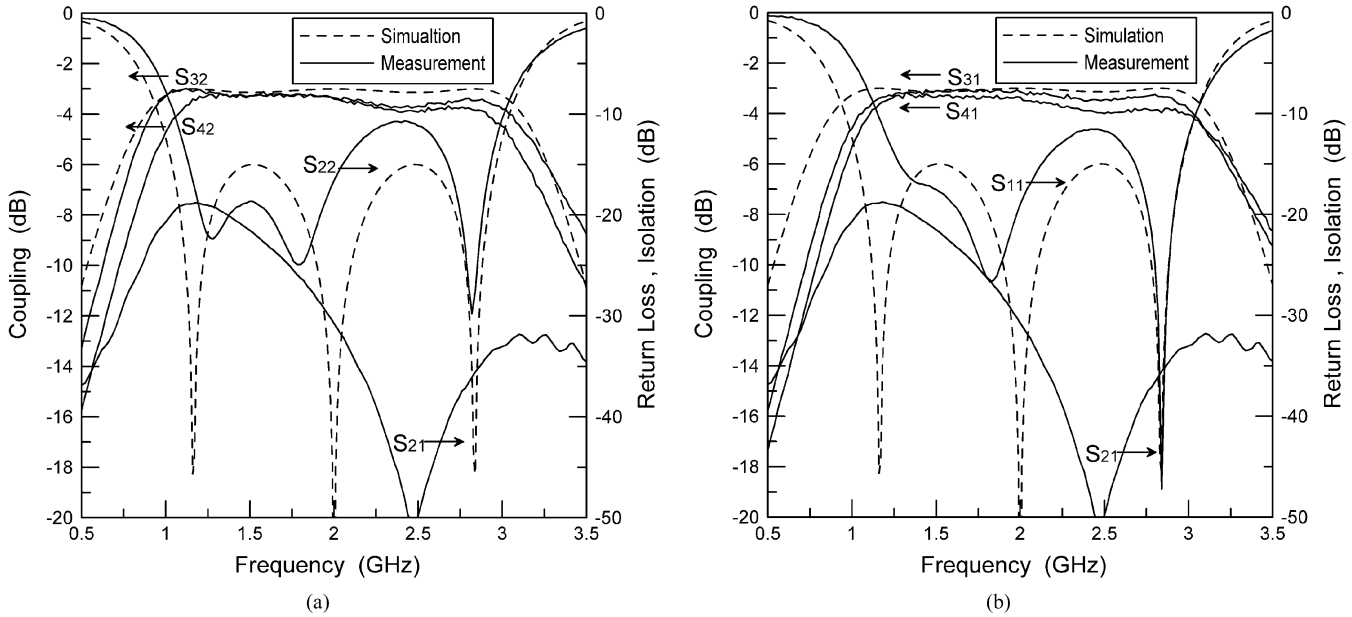

Fig. 13. Measured and simulated results of the 3-dB two-section hybrid ring. (a) Out-of-phase operation. (b) In-phase operation.

According to (7) and (12)–(14), the unknown variables Y_1 and Y_2 can be solved numerically. It should be emphasized that there exists two set of solutions. Let us discuss this in the following.

Fig. 3 shows the plot of characteristic impedances of Z_1, Z_2, and bandwidth versus return loss for the 3-dB two-section hybrid ring shown in Fig. 1(c). The 96.3% bandwidth for return loss better than 15 dB can be achieved. A similar synthesis procedure can be used to solve the unknown variables for the single-section hybrid ring. Fig. 4 shows the plots of characteristic impedances of Z_1, Z_2, and bandwidth versus coupling level, which is defined by the power at the coupling port divided by the incident power, for the single- and two-section hybrid rings with 15-dB return loss. It can be seen that, for the single-section hybrid ring, the bandwidth increases with increasing power-division ratios, but the high impedance value of Z_1 limits the realizable power-division ratios to about -10 dB. The bandwidth of the two-section hybrid ring decreases with increasing of the power-division ratios but the values of Z_1 and Z_2 are both located in the reasonable range for power-division from as strong as -3 dB to weaker than -20 dB.

Fig. 5 shows another set of solutions for the two-section hybrid ring. Comparing with the characteristics of the single-section hybrid ring in Fig. 4, it depicts a larger bandwidth, but requires a higher Z_1 impedance value.

The two-section hybrid ring shown in Fig. 2 comprises two single-section units, where each unit has a unit element at each I/O port. This two-section hybrid ring can achieve larger bandwidth than the above-described two-section hybrid ring. However, the analysis method described above is too complicated to obtain similar design equations. Fortunately, values of unknown variables Y_1, Y_2, Y_3, and Y_4 can be obtained by optimization with the known relationship between Y_1 and Y_2. The design curves for a two-section 3-dB hybrid of this type are shown in Fig. 6.

III. Characteristics of VIP Couplers

Fig. 7 shows the cross-sectional view and the parameters of the VIP coupler. Coupling coefficients can be readily controlled by changing the dielectric constants or the thicknesses of the substrates or the height h and width w of the coupler. Therefore, the newly added vertical substrate can significantly increase the freedom of design. From [7], we know that the electric field is mainly confined in the vertical substrate for odd-mode excitation and in air and main substrate for even-mode excitation.

The equivalent circuit of a short-ended coupled line is shown in Fig. 8 where Z_{0e} and Z_{0o} are the even- and odd-mode characteristic impedances and θ is the electrical length of the coupled line. When $\theta = 90°$, the two shunt-shorted stubs of the characteristic impedance Z_{0e} are open-circuited. Therefore, at the center frequency, the short-ended coupled line is reduced to a $\lambda/4$ transmission line of characteristic impedance $2Z_{0e}Z_{0O}/(Z_{0e} - Z_{0O})$ cascaded with an ideal phase inverter. It should be emphasized that the previously described theory is based on an ideal single-section 180° hybrid ring. However, the two shunt-shorted stubs in Fig. 8 are only open-circuited at the center frequency. Out of the center frequency, the influence of this shunt-shorted stub decreases as the value of Z_{0e} increases. Until Z_{0e} approaches infinity, the short-ended coupled line is equivalent to the phase-inverting arm required in an ideal single-section 180° hybrid ring. To obtain higher Z_{0e}, we can increase the height h of the coupler. Comparing Figs. 1(b) and 8, it can be found that the value of Z_{0o} is close to $Z_2/2$ as long as Z_{0e} is much higher than Z_{0o}. The VIP coupler cannot only realize low values of Z_{0O} but also implement high values of Z_{0e}. Here, the main circuit is fabricated on a RO4003 substrate with 20-mil thickness (h_s) and a dielectric constant (ε_{r1}) of 3.38, and the VIP coupler is implemented on same RO4003 substrate with 8-mil thickness (h_v) and same dielectric constant (ε_{r2}) of 3.38. The characteristic impedances for even- and odd-modes of the VIP couplers can be obtained by the fully three-dimensional

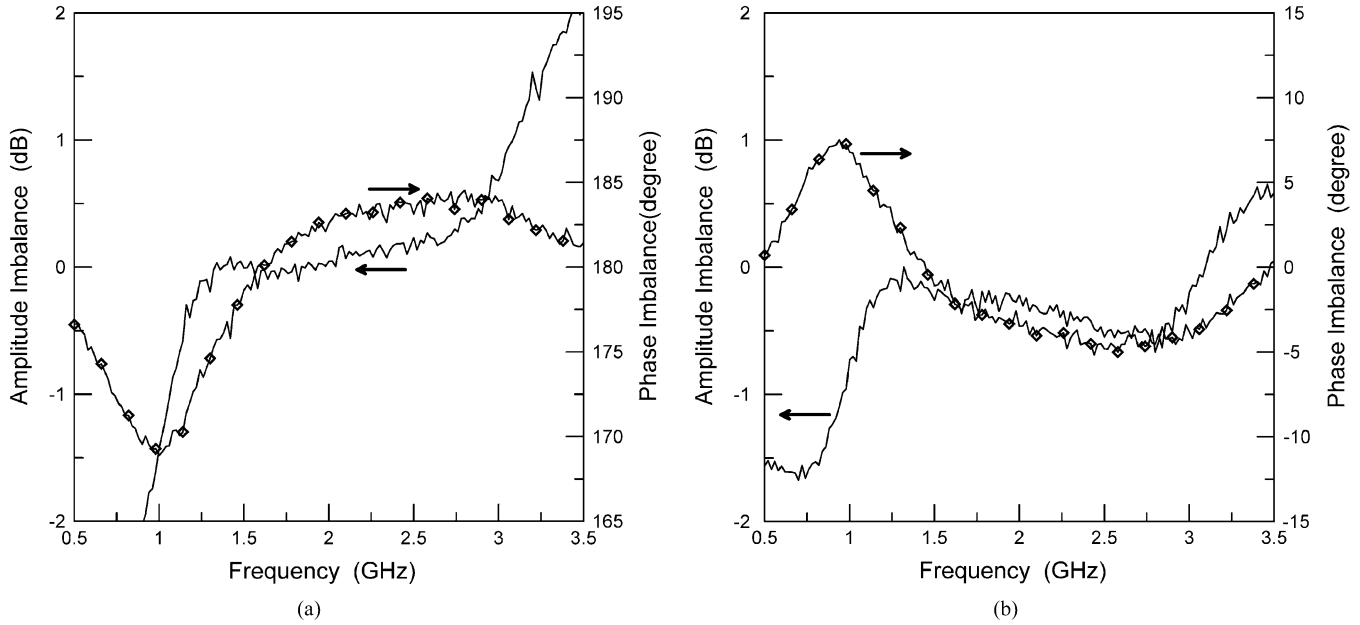

Fig. 14. Measured amplitude and phase imbalances of the 3-dB two-section hybrid ring. (a) Out-of-phase operation. (b) In-phase operation.

(3-D) EM simulator HFSS [11]. Four cases of VIP couplers are calculated for the prototype circuits in the next section. The physical parameters in Fig. 7 and the calculated electrical parameters of the VIP couplers are listed in Table I, where L is the required physical length of the short-ended VIP coupler to provide 270° phase-shifting at the center frequency of 2 GHz. Fig. 9 shows the simulated 15-dB equal-ripple return loss bandwidth of a 3-dB single-section hybrid ring with a short-ended coupler versus different Z_{0e}. It can be seen that the bandwidth approaches an asymptotic value as long as Z_{0e} is higher than about 250 Ω. Therefore, if the VIP coupler can have this high Z_{0e} value, a nearly ideal single-section unit can be implemented. Besides, the VIP coupler can also provide a good crossover in the proposed circuit. Because the signal going through the short-ended VIP coupler is mainly odd-mode and the field of odd-mode is mostly confined in the VIP substrate, the crossover has negligible influence on circuit performance.

IV. Experimental Results And Discussion

As we mentioned previously, the VIP coupler is a good candidate to realize the phase inverter and the crossover on microstrip circuits. Four prototype circuits are fabricated, all with 15 dB of equal-ripple return loss. The four prototype circuits are a single-section reconfigured 3-dB hybrid ring to observe the performance of the single-section building block, a two-section 3-dB hybrid ring with the equivalent circuit shown in Fig. 1(c) to verify the validity of the theory derived in previous section, a two-section 20-dB hybrid ring to show the high power-division ratio of the proposed design in Fig. 1(c), and a two-section 3-dB hybrid ring with the equivalent circuit shown in Fig. 2 to depict the bandwidth extension performance.

The 3-D view of the reconfigured single-section hybrid ring is shown in Fig. 10, and the photograph of the reconfigured and conventional 3-dB hybrid rings is depicted in Fig. 11. The required VIP coupler parameters with $Z = 59\,\Omega$ are also shown in Table I. It can be seen that the reconfigured single-section hybrid ring is compact compared with the conventional one. The measured performance, although not shown, is very close to theoretical results. This is the basic building block of the next three two-section hybrids.

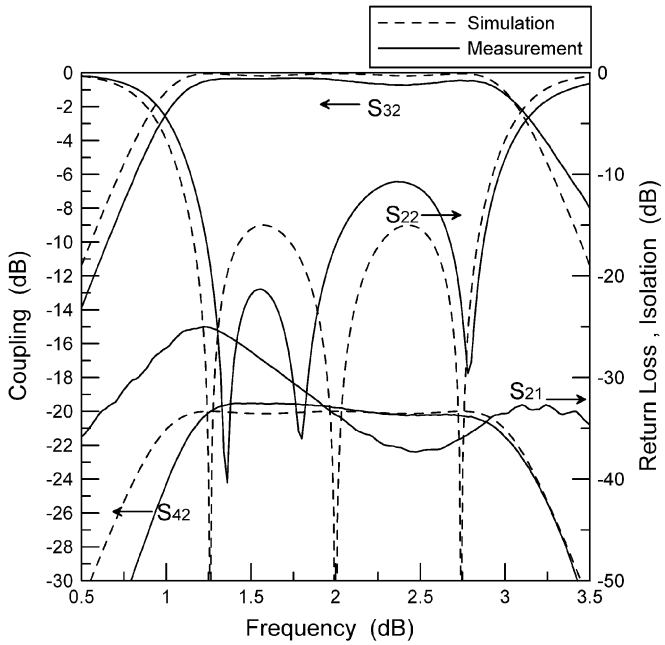

Fig. 15. Measured and simulated results of the 20-dB two-section hybrid ring.

The two-section 3-dB hybrid ring with the equivalent circuit shown in Fig. 1(c) and a photograph shown in Fig. 12(a) has the line impedances of $Z_1 = 99.60\,\Omega$ and $Z_2 = 41.26\,\Omega$. The designed passband is 1.04–2.96 GHz (96% bandwidth). Fig. 13 shows the simulated and measured results and the measured insertion loss is approximately 0.4 dB. The measured return losses are better than 10 dB from 1.06 to 3 GHz for out-of-phase operation and from 1.16 to 3.04 GHz for in-phase operation, respectively. The measured isolation is typically better than 20 dB

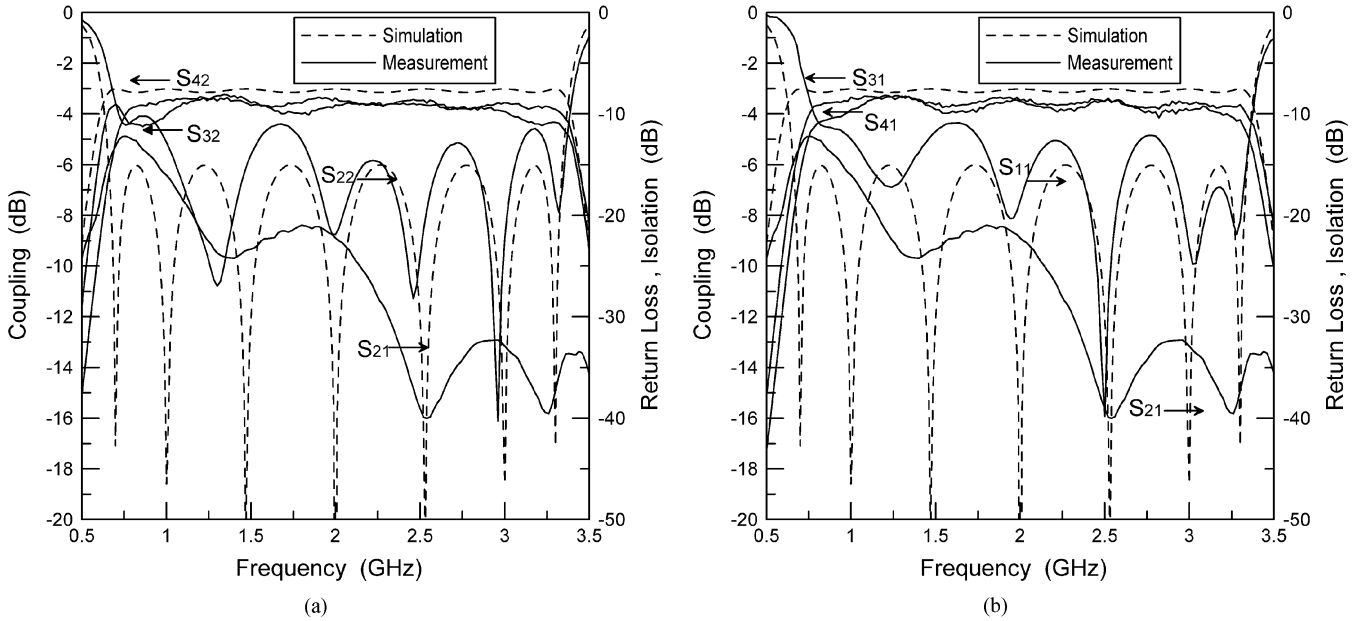

Fig. 16. Measured and simulated results of the 3-dB two-section hybrid ring with a unit element at each I/O port. (a) Out-of-phase operation. (b) In-phase operation.

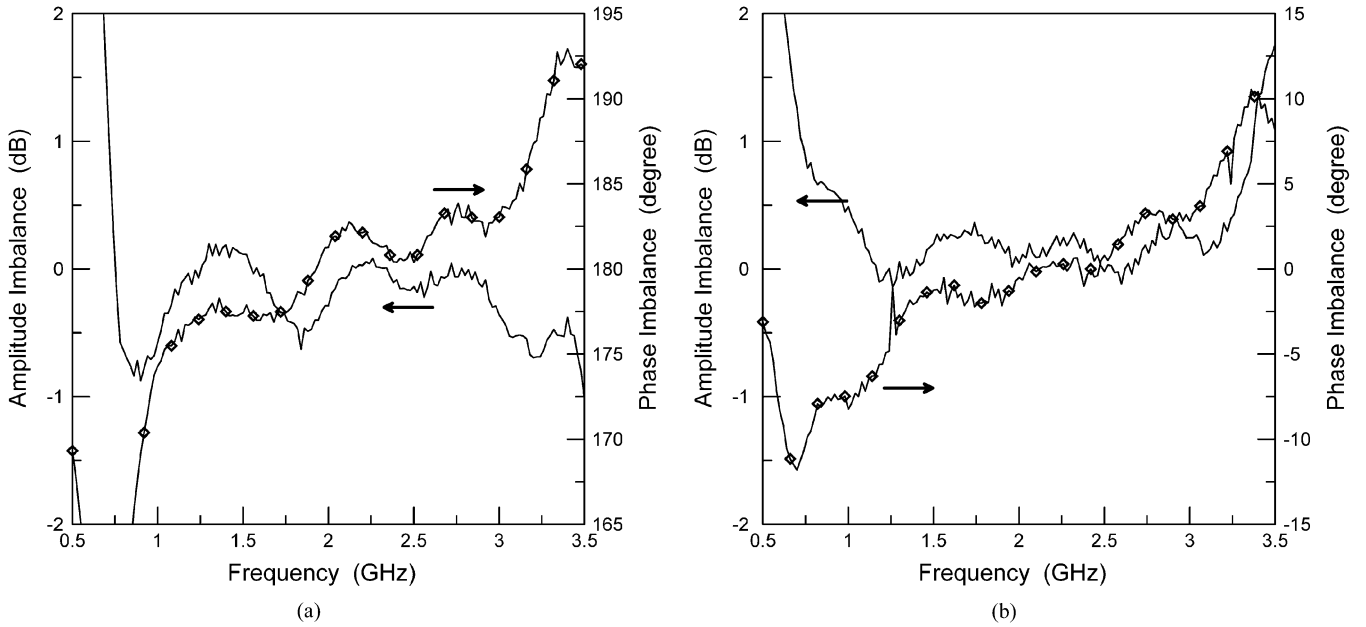

Fig. 17. Measured amplitude and phase imbalances of the 3-dB two-section hybrid ring with a unit element at each I/O port. (a) Out-of-phase operation. (b) In-phase operation.

from 0.5 to 3.5 GHz. The measured amplitude and phase imbalances are shown in Fig. 14. For out-of-phase operation, the amplitude imbalance is within 1 dB from 1.06 to 3.1 GHz and the phase imbalance is within 10° from 1.08 to 3.5 GHz. For in-phase operation, the amplitude imbalance is within 1 dB from 0.96 to 3.5 GHz and the phase imbalance is within 10° from 0.5 to 3.5 GHz. The required VIP coupler parameters with $Z = 41.3\ \Omega$ are shown in Table I.

The two-section 20-dB hybrid ring with the equivalent circuit shown in Fig. 1(c) and a photograph shown in Fig. 12(b) has line impedances of $Z_1 = 56.21\ \Omega$ and $Z_2 = 50.84\ \Omega$. The measured and simulated results are shown in Fig. 15. The designed passband is 1.144–2.856 GHz (85.5% bandwidth). The measured equal-ripple return loss bandwidth is a little narrower than the simulated result. The measured isolation is better than 25 dB from 0.5 to 3.5 GHz. The measured phase performances are not shown here because they are not important for loose coupling. The required VIP coupler parameters with $Z = 50.8\ \Omega$ are shown in Table I. In contrast, a single-section 20-dB hybrid ring with unit element should have $Z_1 = 364.1\ \Omega$, $Z_2 = 36.41\ \Omega$ and $Z_T\,(\text{impedance of a unit element}) = 38.9\ \Omega$ which can hardly be realized by microstrip or CPW circuit. The single-section 20-dB hybrid ring without unit element has higher impedance values that are more difficult to implement.

The two-section 3-dB hybrid ring with the equivalent circuit shown in Fig. 2 and a photograph shown in Fig. 12(c) has the line

impedances of $Z_1 = 71.48\ \Omega, Z_2 = 29.61\ \Omega, Z_3 = 34.29\ \Omega$, and $Z_4 = 29.12\ \Omega$. The designed passband is 0.66–3.34 GHz (134% bandwidth). Fig. 16 shows the simulated and measured results, and the measured insertion loss is approximately 0.6 dB. The measured return losses are better than 10 dB from 0.72 to 3.38 GHz for out-of-phase operation and from 0.82 to 3.36 GHz for in-phase operation, respectively. The measured isolation is better than 20 dB from 1.16 to 3.5 GHz. The measured amplitude and phase imbalances are shown in Fig. 17. For out-of-phase operation, the amplitude imbalance is within 1 dB from 0.72 to 3.5 GHz and the phase imbalance is within 10° from 0.9 to 3.3 GHz. For in-phase operation, the amplitude imbalance is within 1 dB from 0.72 to 3.36 GHz and the phase imbalance is within 10° from 0.76 to 3.38 GHz. The required VIP coupler parameters with $Z = 29.8\ \Omega$ are shown in Table I.

The above measured results indicate the bandwidth of the two-section cascadable hybrid rings using the VIP coupler is a little narrower than that using an ideal phase inverter, especially for in-phase operation. It should be point out that the simulated performances in Figs. 13, 15, and 16 are based on an ideal single-section unit. The bandwidth shrinkage is due to the fact that the infinity value of Z_{0e} is impractical to be fabricated. In previous section, we have shown that if the Z_{0e} higher than 250 Ω, the performance of a single-section unit approaches an ideal hybrid ring. Nevertheless, the characteristics of a single-section unit equal to those of an ideal hybrid ring only when Z_{0e} is infinity. Therefore, the bandwidth is shrunk due to finite Z_{0e} especially in the cascaded case. In addition, the junction effect (especially junctions at microstrip and VIP coupler) and circuit fabricating imperfections degrade the bandwidth further.

V. Conclusion

In this paper, by reconfiguring the ideal single-section hybrid ring, the wideband two-section hybrid rings with Chebyshev characteristics have been developed for bandwidth enhancement, size reduction, and high power-division ratios. Design equations and design curves have been presented. Using these design curves, the two-section hybrid rings of any power-division ratio can be readily realized. In addition, the two-section hybrid ring by cascading of two single-section unit with a unit element at each I/O port is presented for further bandwidth improvement. The short-ended VIP coupler has been successfully used to approach an ideal single-section unit. It also provides a good crossover for realization of the circuit. Thus, the wideband multisection hybrid rings using the VIP coupler are suitable for microstrip implementation. The measured results show good agreements with the simulated responses.

References

[1] S. March, "A wideband stripline hybrid ring," *IEEE Trans. Microw. Theory Tech.*, vol. MTT-16, no. 6, p. 361, Jun. 1968.

[2] S. Rehnmark, "Wide-band balanced line microwave hybrids," *IEEE Trans. Microw. Theory Tech.*, vol. MTT-25, no. 10, pp. 825–830, Oct. 1977.

[3] C. Y. Chang and C. C. Yang, "A novel broad-band chebyshev-response rat-race ring coupler," *IEEE Trans. Microw. Theory Tech.*, vol. 47, no. 4, pp. 455–462, Apr. 1999.

[4] A. K. Agrawal and G. F. Mikucki, "A printed circuit hybrid-ring directional coupler for arbitrary power divisions," *IEEE Trans. Microw. Theory Tech.*, vol. MTT-34, no. 12, pp. 1401–1407, Dec. 1986.

[5] K. S. Ang, Y. C. Leong, and C. H. Lee, "A new class of multisection 180° hybrids based on cascadable hybrid-ring couplers," *IEEE Trans. Microw. Theory Tech.*, vol. 50, no. 9, pp. 2147–2152, Sep. 2002.

[6] R. Levy and L. F. Lind, "Synthesis of symmetrical branch-guide directional couplers," *IEEE Trans. Microw. Theory Tech.*, vol. MTT-16, no. 2, pp. 80–89, Feb. 1968.

[7] Y. Konishi, I. Awai, Y. Fukuoka, and M. Nakajima, "A directional coupler of a vertically installed planar circuit structure," *IEEE Trans. Microw. Theory Tech.*, vol. 36, no. 6, pp. 1057–1063, Jun. 1988.

[8] J. A. Dobrowolski, *Introduction to Computer Methods for Microwave Circuit Analysis and Design*. Norwood, MA: Artech House, 1991, pp. 81–90.

[9] H. J. Riblet, "The application of a new class of equal-ripple functions to some familiar transmission-line problems," *IEEE Trans. Microw. Theory Tech.*, vol. MTT-12, no. 7, pp. 415–421, Jul. 1964.

[10] H. J. Carlin and W. Kohler, "Direct synthesis of band-pass transmission line structures," *IEEE Trans. Microw. Theory Tech.*, vol. MTT-13, no. 5, pp. 283–297, May 1965.

[11] HFSS. ver. 9.2, Ansoft, Pittsburgh, PA, 2004.

Chun-Hsiang Chi was born in Kaohsiung, Taiwan, R.O.C., on August 13, 1980. He received the B.S. degree in electrical engineering from the National Sun Yat-Sen University, Kaohsiung, Taiwan, R.O.C., in 2002, the M.S. degree in communication engineering from the National Chiao-Tung University, Hsinchu, Taiwan, R.O.C., in 2004, and is currently working toward the Ph.D. degree in communication engineering at the National Chiao Tung University.

His research interests include the analysis and design of microwave and millimeter-wave circuits.

Chi-Yang Chang (S'88–M'95) was born in Taipei, Taiwan, R.O.C., on December 20, 1954. He received the B.S. degree in physics and the M.S. degree in electrical engineering from National Taiwan University, Taipei, Taiwan, R.O.C., in 1977 and 1982, respectively, and the Ph.D. degree in electrical engineering from the University of Texas at Austin, in 1990.

From 1979 to 1980, he was with the Department of Physics, National Taiwan University as a Teaching Assistant. From 1982 to 1988, he was with the Chung-Shan Institute of Science and Technology (CSIST), as an Assistant Researcher, where he was in charge of development of MICs, microwave subsystems, and millimeter-wave waveguide E-plane circuits. From 1990 to 1995, he was with CSIST as an Associate Researcher, where he was in charge of development of uniplanar circuits, ultra-broadband circuits, and millimeter-wave planar circuits. In 1995, he joined the faculty of the Department of Communication, National Chiao-Tung University, Hsinchu, Taiwan, R.O.C., as an Associate Professor and became a Professor in 2002. His research interests include microwave and millimeter-wave passive and active circuit design, planar miniaturized filter design, and MMIC design.